MAGNETIC FIELD SUPPRESSION OF MELT FLOW IN CRYSTAL GROWTH

Brian H. Dennis and George S. Dulikravich
Department of Mechanical and Aerospace Engineering, UTA Box 19018
The University of Texas at Arlington, Arlington, Texas 76019, USA

ABSTRACT. The p-version least-squares finite element method was used for prediction of solidification from a melt under the influence of an externally applied magnetic field. The computational results indicate significantly different flow-field patterns and thermal fields in the melt and the accrued solid in the cases of full gravity, reduced gravity, and an applied uniform magnetic field. This clearly suggests the possibility of optimizing magnetic field distribution and crucible shapes for controlling the melt recirculation.

INTRODUCTION

When growing a crystal, such as a semiconductor crystal, it is desirable to remove the thermally induced convection effects entirely, leading to heat transfer by pure conduction. This is good for two reasons. First, if the velocity within the melt region is high, it is more likely that small particles of the crucible wall will be deposited in the crystal [1]. Such contamination dramatically reduces the quality of the solid crystal. Second, for some semiconductors, a dopant is introduced into the melt. It is desirable to achieve a distribution of the dopant in the solid crystal that is as uniform as possible [2]. This is easier to realize under pure heat conduction with no convection [2].

One way to reduce the convection in the melt region is to perform the crystal growth in a low gravity environment, such as in an Earth-orbiting vehicle. Since semiconductor melts are highly electrically conducting, a more practical approach is to use magnetic and electric fields to suppress the buoyancy induced flows. With such an electromagnetic device, high quality crystals can be produced under full gravity.

Magnetic fields can be used to damp the convection during the directional solidification of electrically conductive melts [3]. Computational methods are needed to enhance our understanding of the phenomena occurring during the solidification of semiconductor melts. Effects like the bending of isomagnetic lines and the effects of different crucible shapes on the melt flow are difficult to model analytically and so they may be studied numerically. In addition, numerical simulation can be used together with optimization to determine the distributions of the magnetic field lines and the shape of the crucible that will minimize the convective flow throughout the melt.

The equations for laminar steady-state incompressible Newtonian magnetohydrodynamic flows with the Boussinesq approximation [4] can be written in the following non-dimensional form [5, 6]:

$$\nabla \cdot \mathbf{V}^* = 0 \quad (1)$$

$$\rho^* \mathbf{V}^* \cdot \nabla \mathbf{V}^* - \tfrac{1}{Re} \nabla \cdot \left(\eta^* \left(\nabla \mathbf{V}^* + (\nabla \mathbf{V}^*)^T \right) \right) + \nabla p^* - \rho^* \tfrac{Ht^2}{Re} \mathbf{V}^* \times \mathbf{B}^* \times \mathbf{B}^* - \rho^* \tfrac{1}{Fr} \mathbf{k} T^* = 0 \quad (2)$$

$$\rho^* Cp^* \mathbf{V}^* \cdot \nabla T^* - \frac{1}{Pe}\nabla \cdot (k^* \nabla T^*) - \frac{Ht^2 Ec}{Re}(\mathbf{V}^* \times \mathbf{B}^*)^2 = 0 \quad (3)$$

$$\nabla \cdot \mathbf{B}^* = 0 \quad (4)$$

$$\nabla^* \times \mathbf{B}^* - Rm \mathbf{V}^* \times \mathbf{B}^* = 0 \quad (5)$$

where $\mathbf{V}^*$ is the fluid velocity, ρ^* is the fluid density, p^* is the hydrodynamic pressure, η^* is the temperature dependent coefficient of viscosity, $\mathbf{B}^*$ is the magnetic flux density. Only the presence of a steady magnetic field is considered here so the equations and terms in Maxwell's equations relating to the electric field are omitted. The non-dimensional variables are defined as $\mathbf{V}^* = \mathbf{V}\, U_0^{-1}$, $\mathbf{B}^* = \mathbf{B}\, B_0^{-1}$, $p^* = p\, \rho_0^{-1} U_0^{-2}$, $x^* = x\, L_0^{-1}$, $y^* = y\, L_0^{-1}$,$\rho^* = \rho\, \rho_0^{-1}$,$\eta^* = \eta\, \eta_0^{-1}$,$Cp^* = Cp\, Cp_0^{-1}$, and $T^* = \frac{T - T_{cold}}{\Delta T_0}$. The vector $\mathbf{k}$ is the unit normal in the y direction. The temperature is nondimensionalized with a temperature difference, ΔT_0, where $\Delta T_0 = T_{hot} - T_{cold}$. The nondimensional numbers are given by:

Reynolds number: $Re = \dfrac{\rho_0 U_0 L_0}{\eta_0}$ Hartmann number: $Ht = L_0 B_0 \sqrt{\dfrac{\sigma_0}{\eta_0}}$

Froude number: $Fr = \dfrac{U_0^2}{\Delta T_0 \beta_0 g_0 L_0}$ Magnetic Reynolds number: $Rm = \mu_0 \sigma_0 U_0 L_0$

Peclet number: $Pe = \dfrac{L_0 U_0 \rho_0 Cp_0}{k_0}$ Eckert number: $Ec = \dfrac{U_0^2}{Cp_0 \Delta T_0}$

where Cp_0 is the specific heat, k_0 is the heat conductivity coefficient, β_0 is the volumetric thermal expansion coefficient, g_0 is the acceleration of gravity, μ_0 is the magnetic permeability coefficient, and σ_0 is the electrical conductivity of the fluid.

In this paper, the growth of a silicon crystal under an applied magnetic field has been simulated with the p-version of the least-squares finite element method (LSFEM) [7, 8] for magnetohydrodynamics (MHD) [9, 10, 11]. The solidification is modeled by using temperature dependent properties. The material properties for silicon are given in Table 1. Here L is the latent heat of liquid/solid phase change. The subscripts l and s refer to the liquid and solid properties, respectively. In the mushy region (where $T_l > T > T_s$), the density, specific heat, latent heat,

Table 1: Parameters for MHD silicon crystal growth problem

Density of the melt	$\rho_l(kgm^{-2})$	2550.0
Density of the solid	$\rho_s(kgm^{-2})$	2330.0
Length of the container	Length (m)	0.10
Heat conductivity of the melt	$k_l(Wkg^{-1}K^{-1})$	64.0
Heat conductivity of the solid	$k_s(Wkg^{-1}K^{-1})$	22.0
Liquidus temperature	$T_l(K)$	1685.0
Solidus temperature	$T_s(K)$	1681.0
Specific heat of the melt	$C_{p_l}(Jkg^{-1}K^{-1})$	1059.0
Specific heat of the solid	$C_{p_s}(Jkg^{-1}K^{-1})$	1038.0
Viscosity of the melt	$\eta(kgm^{-1}s^{-1})$	0.0007
Electric conductivity	$\sigma(\Omega^{-1}m^{-1})$	4.3×10^4
Latent heat of phase change	$L(Jkg^{-1})$	1.8×10^6
Thermal expansion coefficient	$\beta(K^{-1})$	1.4×10^{-4}

and the viscosity were taken as linear functions of temperature.

$$f = \frac{T - T_s}{T_l - T_s} \quad (6)$$

$$\rho = f\rho_l + (1-f)\rho_s \quad (7)$$
$$\eta = f\eta_l + (1-f)\eta_s \quad (8)$$
$$C_p = fC_{p_l} + (1-f)C_{p_s} \quad (9)$$

The solid regions are modeled as a melt with a high viscosity ($\eta_s = 10^3\, kg\, m^{-1} s^{-1}$) [6]. Consequently, the computed velocities in the solid regions are not identically zero, but are extremely small compared to the velocities in the melt. This formulation allows one code to simultaneously simulate heat transfer through solid, melt, and mushy regions.

The effect of the latent heat, L, is included by using an enthalpy method [12]. Typically, the effect of the latent heat can be included in a numerical simulation by allowing a rapid variation in the heat capacity in the mushy region. This direct evaluation leads to satisfactory numerical integrations only if the curve of the heat capacity against the temperature does not possess sharp peaks. If the mushy region is completely contained within a single element, there is a chance that it may not fall on an integration point and hence the latent heat will not be accounted for in the integration process. A better approach is work with enthalpy, H, which is a smooth function even in the phase change zone. The effective heat capacity can be evaluated without missing the peaks due to the latent heat. The relation

$$\rho C_p = \frac{dH}{dT} \quad (10)$$

is approximated by

$$\rho C_p \approx \frac{\sqrt{(\partial H/\partial x)^2 + (\partial H/\partial y)^2}}{\sqrt{(\partial T/\partial x)^2 + (\partial T/\partial y)^2}} \quad (11)$$

in an attempt to avoid the possibility of missing the peak values ρC_p during the numerical integration procedure.

NUMERICAL METHOD

The p-version LSFEM [13] was implemented in this work. Details have been published recently by the authors [14]. The p-type finite elements were developed using hierarchical basis functions based on Jacobi polynomials [15]. The hierarchical basis leads to a linear algebraic system with a natural multilevel structure that is well suited to adaptive enrichment. The sparse linear systems were solved by either direct sparse LU factorization or by iterative methods. Two iterative methods were implemented in the software, one based on a Jacobi preconditioned conjugate gradient and the another based a multigrid-like technique that uses the hierarchy of basis functions instead of a hierarchy of finer grids. The method was implemented in an object-oriented fashion using the C++ programming language. The software has been tested against analytic solutions and experimental data for Navier-Stokes equations and for channel flows through transverse electric and magnetic fields, for shear-driven cavity flows, buoyancy-driven cavity flows, and flow over a backward-facing step [14].

VERIFICATION OF ACCURACY

The accuracy of the LSFEM for MHD was tested against known analytic solutions for Poisuille-Hartmann flow. The Poisuille-Hartmann flow is a 1-D flow of a conducting and viscous fluid between two stationary plates with a uniform external magnetic field applied orthogonal to the plates. An analytical solution to the equations governing MHD can be found for this case [5].

The Hartmann flow problem has been computed using the p-version LSFEM method for MHD. A mesh composed of four quadrilateral elements is used with a uniform p-level of $P = 8$ for

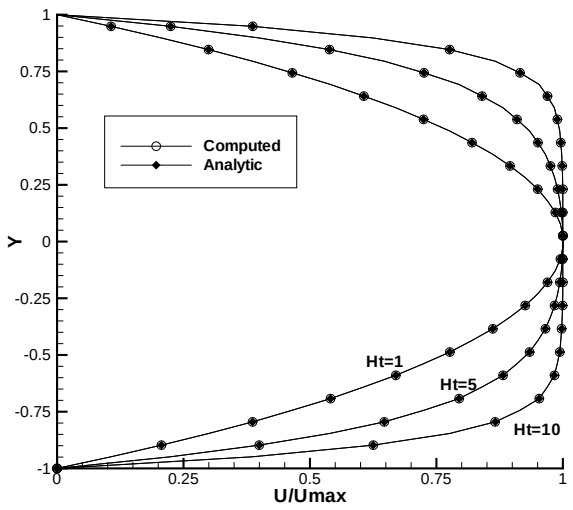

Figure 1: Computed velocity profiles for Hartmann flow for various values of Ht

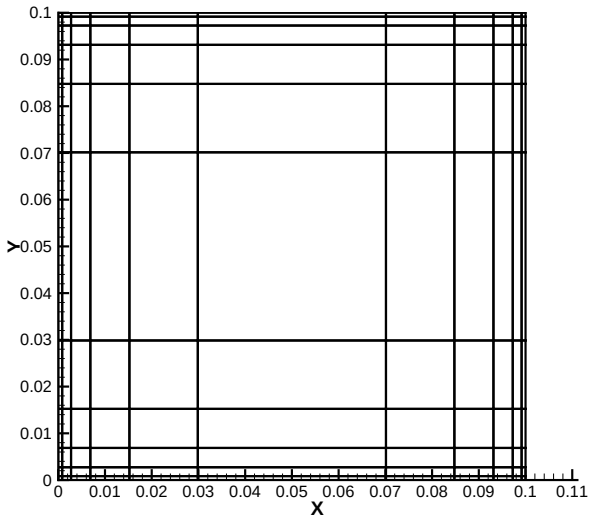

Figure 2: Mesh from crystal growth problem

all cases. Figure 1 shows the change in the u velocity for different values of Hartmann number for both the analytic solution and the computed solution. Larger values of Hartmann number, Ht, correspond to larger magnetic field strengths. Excellent agreement is obtained between the computed and analytic solutions for the range of Hartmann numbers.

NUMERICAL RESULTS

The solidification of a silicon crystal in a square container both with and without an applied magnetic field has been simulated. The container sides have the length of $0.1\,m$. The solidification occurs on the top wall of the container. The side walls are thermally insulated. A parabolic temperature profile is applied to the bottom of the container to simulate nonuniform heating of the melt. The temperature at the center of the bottom wall is $1688.0\,K$ and the temperature at the bottom corners is set to $1686.0\,K$. A uniform temperature of $1676.0\,K$ is applied to the top wall. A no-slip condition for velocity is enforced on all walls of the container. A quadrilateral mesh with 121 elements with a p-level of $P = 6$ is used for all cases. The mesh is shown in figure 2. A uniform vertical magnetic field is applied to container by placing magnets on the top and bottom walls and using a perfect conductor on the side walls.

Three test cases have been simulated. In all cases gravity acts in the y direction and is therefor aligned with the magnetic field. In all the cases the steady-state solution to the equations governing MHD with heat transfer is predicted. The relevant non-dimensional and dimensional parameters for these test cases problem are shown in Table 2 .

The first case uses full gravity, $g = 9.81\,m\,s^{-2}$ with an applied magnetic field strength of $B_0 = 0.0\,T$. Figure 5 shows the resulting streamlines within the melt region. Two pairs of counter rotating vortices are present within the melt region. Figure 4 shows the computed

Table 2: Relevant dimensional and non-dimensional parameters for the three test cases

Test Case	$g\,(ms^{-2})$	$B_0\,(T)$	Re	Pe	Ra	Pr	Ht
1	9.81	0.0	4269.14	49.4487	211103	0.01158	0.0
2	0.1	0.0	431.029	4.99252	2151.92	0.01158	0.0
3	9.81	1.0	4269.14	49.4487	211103	0.01158	783.764

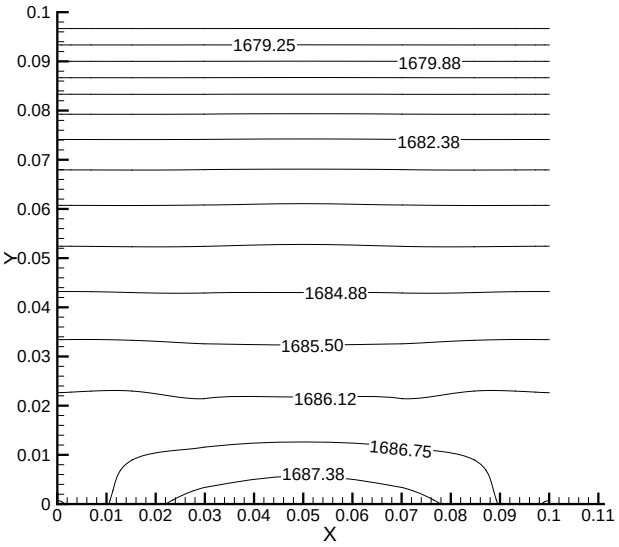

Figure 3: Computed temperature contours for $g = 9.81\,m\,s^{-2}$ and $B_0 = 0.0\,T$

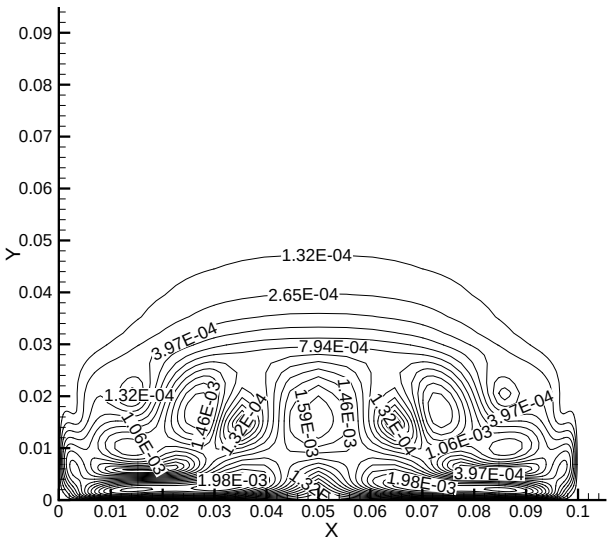

Figure 4: Computed velocity magnitude for $g = 9.81\,m\,s^{-2}$ and $B_0 = 0.0\,T$

velocity magnitude within the melt region. The maximum velocity is $0.0021\,2m\,s^{-1}$ and occurs around $x = 0.05\,m$ and $y = 0.015\,m$. The computed temperature distribution is shown in Figure 3. The motion of the melt results in a temperature distribution that is different from that obtained under pure diffusion.

The second case uses reduced gravity, $g = 0.10\,m\,s^{-2}$ with an applied magnetic field strength of $B_0 = 0.0\,T$. Such an environment would exist if the crystal were growth in an Earth-orbiting satellite. Figure 6 shows the resulting streamlines within the melt region. Two pairs of counter rotating vortices are present within the melt region. In this case, the vortices are weaker than in the first case. Figure 8 shows the computed velocity magnitude within the melt region. The maximum velocity is $0.000172\,m\,s^{-1}$ and occurs around $x = 0.05\,m$ and $y = 0.015\,m$. The computed temperature distribution is shown in Figure 7. The temperature distribution is very similar to that obtained under pure diffusion.

The last case uses full gravity, $g = 9.81\,m\,s^{-2}$ with an applied magnetic field strength of $B_0 = 1.0\,T$. Figure 9 shows the resulting streamlines within the melt region. Only one pair of counter rotating vortices are present within the melt region. The magnetic field has completely suppressed the secondary vortices that were present in the cases without the magnetic field. Figure 11 shows the computed velocity magnitude within the melt region. The maximum velocity is $0.0000434\,m\,s^{-1}$ and occurs around $x = 0.05\,m$ and $y = 0.018\,m$. The computed temperature distribution is shown in Figure 10. The temperature distribution is very similar to that obtained under pure diffusion. This case demonstrates that buoyancy induced flow velocities can be significantly reduced through the use of applied magnetic fields.

It should be noted that in this analysis it is assumed that the solid and the liquid regions have the same electrical conductivity. In the real case, the electrical conductivity may vary significantly between the solid and liquid phases. This change in conductivity would result in the bending of the magnetic field lines though the mushy region [3]. The present LSFEM algorithm would need to be modified to include a front tracking algorithm in order to accurately account for this effect.

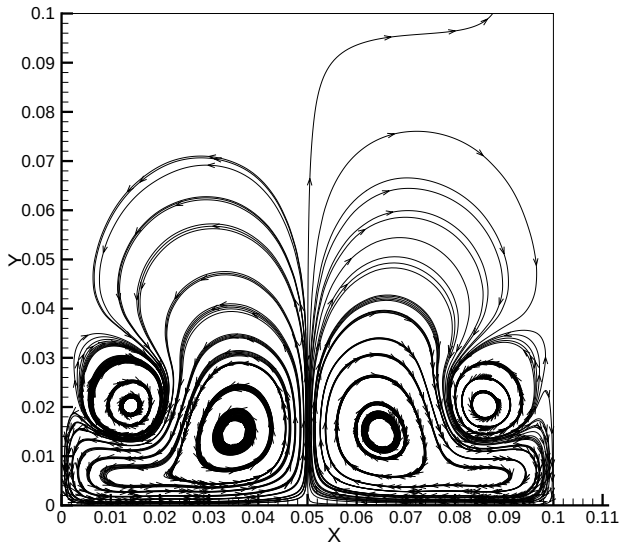

Figure 5: Computed streamlines for $g = 9.81\,m\,s^{-2}$ and $B_0 = 0.0\,T$

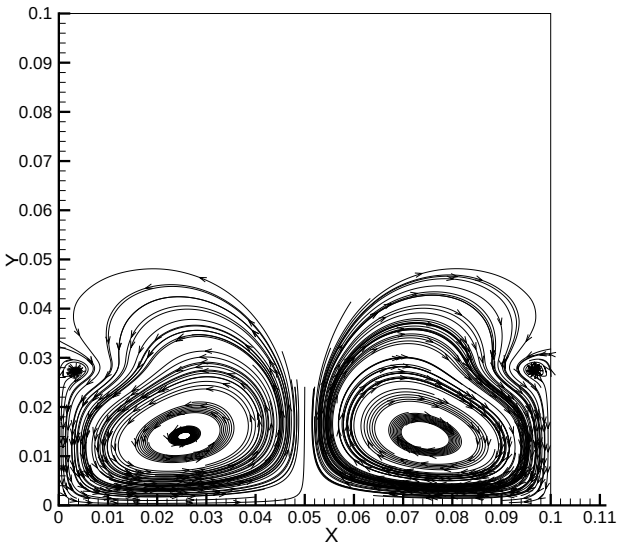

Figure 6: Computed streamlines for $g = 0.01\,m\,s^{-2}$ and $B_0 = 0.0\,T$

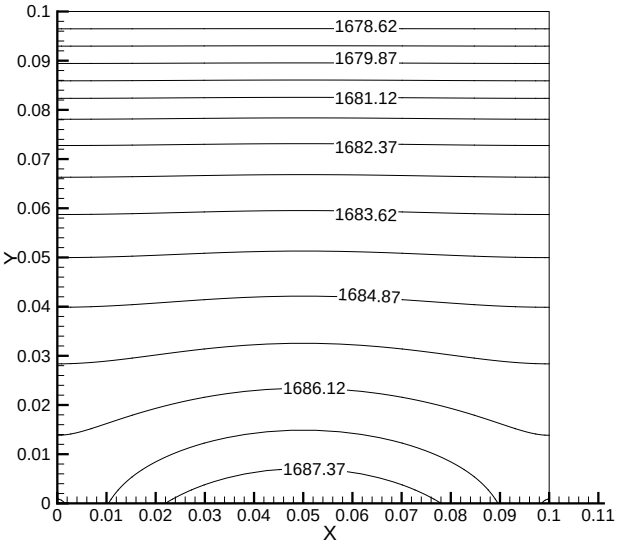

Figure 7: Computed temperature contours for $g = 0.01\,m\,s^{-2}$ and $B_0 = 0.0\,T$

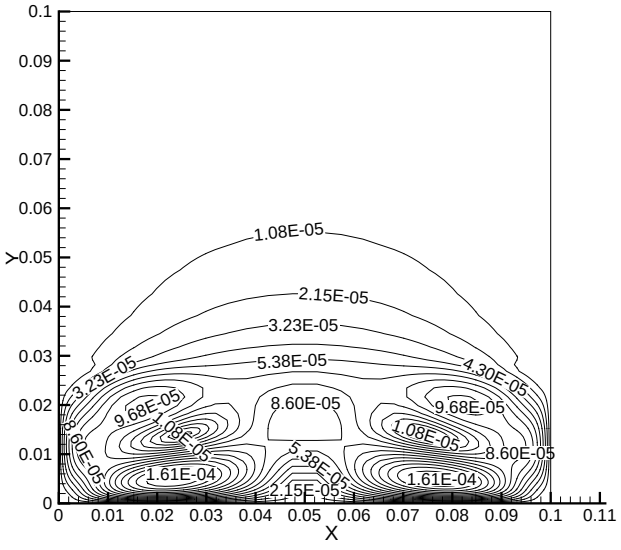

Figure 8: Computed velocity magnitude for $g = 0.01\,m\,s^{-2}$ and $B_0 = 0.0\,T$

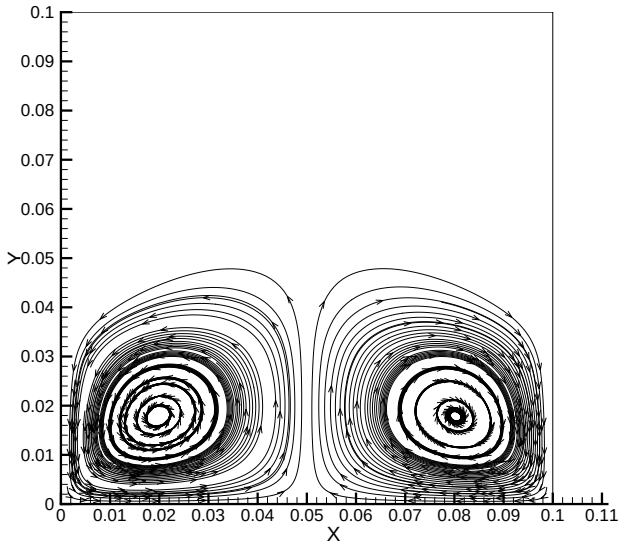

Figure 9: Computed streamlines for $g = 9.81\,m\,s^{-2}$ and $B_0 = 1.0\,T$

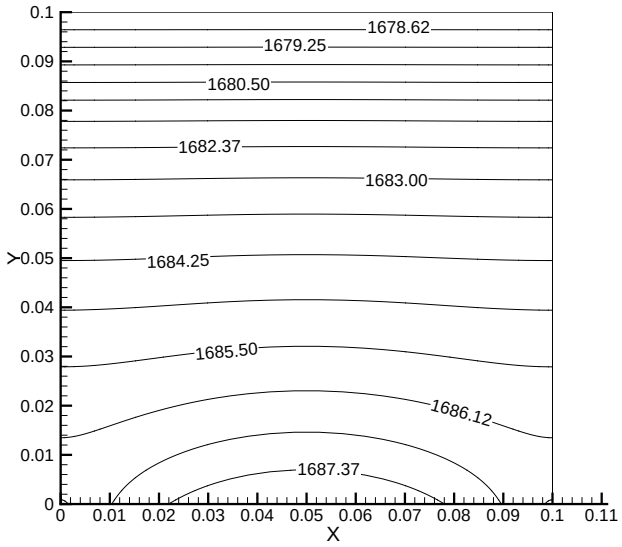

Figure 10: Computed temperature contours for $g = 9.81\,m\,s^{-2}$ and $B_0 = 1.0\,T$

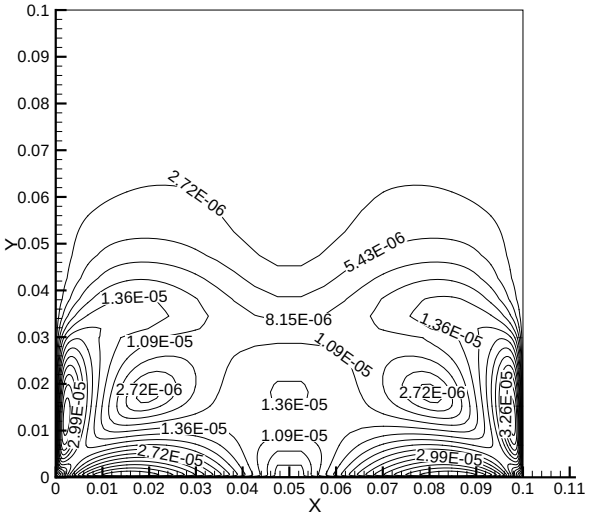

Figure 11: Computed velocity magnitude for $g = 9.81\,m\,s^{-2}$ and $B_0 = 1.0\,T$

CONCLUSIONS AND RECOMMENDATIONS

The p-version least-squares finite element method was successfully used for the prediction of solidification from a melt under an externally applied uniform magnetic field. The computational results indicate significantly different flow-field patterns and thermal fields in the melt and the accrued solid in the cases of full gravity, reduced gravity, and an applied uniform magnetic field. Although the magnetic field significantly reduces the velocity of the flow within the melt, the crystal may still be slightly contaminated. It is desirable to completely eliminate the motion within the melt. It is possible that a uniform magnetic field much stronger than $1.0\,T$ may be required. Such magnets require superconducting ceramics and are costly to maintain. It may be possible to use the current LSFEM based software for MHD together with numerical optimization software to optimize the shape of the container as well as the distribution of the magnetic field along the container wall. Such optimized configurations may locally eliminate motion in the melt with lower strength magnets.

REFERENCES

[1] Garandet, J. P. and Alboussiere, T., *Bridgman Growth: Modeling and experiments*, Pergamon Press, to appear.

[2] Hirtz, J. M. and Ma, N., "Dopant transport during semiconductor crystal growth: axial versus transverse magnetic fields," *Journal of Crystal Growth*, Vol. 210, 2000, pp. 554–572.

[3] Fedoseyev, A. I., Kansa, E. J., Marin, C., and Ostrogorsky, A. G., "Magnetic Field Suppression of Semiconductor Melt Flow in Crystal Growth: Comparison of Three Methods for Numerical Modeling," *CFD Journal*, 2000.

[4] Gray, D. D. and Giorgini, A., "The Validity of the Boussinesq Approximation for Liquids and Gases," *Int. J. Heat and Mass Transfer*, Vol. 19, 1976, pp. 175–189.

[5] Hughes, W. F. and Young, F. J., *The Electromagnetodynamics of Fluids*, John Wiley and Sons, New York, 1966.

[6] Dulikravich, G. S., Ahuja, V., and Lee, S., "Modeling Three-Dimensional Solidification With Magnetic Fields and Reduced Gravity," *International Journal of Heat and Mass Transfer*, Vol. 37, No. 5, 1994, pp. 837–853.

[7] Jiang, B.-N., *The Least-Squares Finite Element Method*, Spring-Verlag, Berlin, 1998.

[8] Bochev, P. B., "Analysis of Least-squares Finite Element Methods for Navier-Stokes Equations," *SIAM Journal of Numerical Analysis*, Vol. 34, No. 5, 1997, pp. 1817–1844.

[9] Dulikravich, G. S., "Electro-Magneto-Hydrodynamics and Solidification," *Advances in Flow and Rheology of Non-Newtonian Fluids, Part B*, edited by D. A. Siginer, D. D. Kee, and R. P. Chhabra, Vol. 8 of *Rheology Series*, chap. 9, Elsevier Publishers, 1999, pp. 677–716.

[10] Dennis, B. H. and Dulikravich, G. S., "Simulation of Magnetohydrodynamics With Conjugate Heat Transfer," *European Congress on Computational Methods in Applied Sciences and Engineering*, edited by E. Onate, September 11-14, 2000, Barcelona, Spain.

[11] Dennis, B. H. and Dulikravich, G. S., "Optimization of Magneto-Hydrodynamic Control of Diffuser Flows Using Micro-Genetic Algorithm and Least Squares Finite Elements," *Journal of Finite Elements in Finite Elements in Design*, in press.

[12] Morgan, K., Lewis, R. W., and Zienkiewicz, O. C., "An Improved Algorithm for Heat Conduction and Problems with Phase Change," *International Journal for Numerical Methods in Engineering*, 1977, pp. 1191–1195.

[13] Jiang, B.-N. and Sonnad, V., "Least-Squares Solution of Incompressible Navier-Stokes Equations with the p-Version of Finite Elements," *Computational Mechanics*, Vol. 15, 1994, pp. 129–136.

[14] Dennis, B. H., *Simulation and Optimization of Electromagnetohydrodynamic Flows*, Ph.D. thesis, Pennsylvania State University, University Park, PA, Dec. 2000.

[15] Karniadakis, G. E. and Sherwin, S. J., *Spectral/hp Element Methods for CFD*, Oxford University Press, New York, 1999.